

## Optimization of Al<sub>2</sub>O<sub>3</sub>/PES membranes for wastewater filtration

Nermen Maximous, G. Nakhla\*, K. Wong, W. Wan

*Department of Chemical and Biochemical Engineering, Faculty of Engineering, University of Western Ontario, 1151 Richmond Street, London, Ontario, Canada N6A 5B9*

### ARTICLE INFO

#### Article history:

Received 17 September 2009

Received in revised form 16 April 2010

Accepted 16 April 2010

#### Keywords:

Al<sub>2</sub>O<sub>3</sub>

Nanoparticles

Membrane bioreactors

Fouling

Activated sludge

### ABSTRACT

In this study, polyethersulfone (PES) ultrafiltration membranes were casted and modified by dispersing nano-sized alumina (Al<sub>2</sub>O<sub>3</sub>) particles uniformly in a PES solution (18% polymer weight). Membranes with 5 different weight ratios of Al<sub>2</sub>O<sub>3</sub> to PES of 0.01, 0.03, 0.05, 0.1, and 0.2 were examined. Ultrafiltration experiments compared water flux and molecular weight cut-offs (MWCO) for the wet membranes. The effects of the nanometer Al<sub>2</sub>O<sub>3</sub>-particles concentration in the polymer dope on the permeation properties, membrane strength, and anti-fouling performance were examined using activated sludge. The membrane matrix was characterized using scanning electron microscope (SEM). Al<sub>2</sub>O<sub>3</sub> entrapped membranes showed lower flux decline compared to neat polymeric membranes. Fouling mitigation initially increased with nanoparticle content and stabilized thereafter. The optimum load of Al<sub>2</sub>O<sub>3</sub> immobilized membranes for MBR application in terms of highest membrane permeability and lowest fouling rate was the 5% weight fraction of Al<sub>2</sub>O<sub>3</sub> with PES.

© 2010 Elsevier B.V. All rights reserved.

### 1. Introduction

The use of membrane bioreactors (MBRs), for wastewater treatment has been rapidly increasing recently due to superior performance and significant reductions in membrane costs. However, membrane filtration performance inevitably decreases with filtration time due to membrane fouling. More severe fouling is expected when hydrophobic membranes are used in the MBR. The preparation of novel organic-inorganic composite membranes with controlled properties has been a point of considerable interest over the last decade. The presence of finely dispersed inorganic particles in the polymer matrix has proven very useful in the improvement of membrane performance for a wide spectrum of processes, ranging from gas separation and pervaporation to nano- and ultrafiltration [1–5]. Moreover, by the way of blending, the modified membrane can combine basic properties of organic and inorganic materials and offer specific advantages with respect to separation performances, thermal and chemical resistance, and adaptability to the harsh wastewater environments [6–8]. Several types of inorganic materials have been blended with polyvinylidene fluoride (PVDF) such as silica [9], zirconium dioxide (ZrO<sub>2</sub>) [10], Al<sub>2</sub>O<sub>3</sub> [11] and some low molecular weight inorganic salts, such as lithium salts [12]. TiO<sub>2</sub> nanoparticles have also been used in water treatment membranes recently [6–8]. Molinari et al. [6–8] reported on the promise of photocatalytic membrane reactors for

toxic organic removal using immobilized TiO<sub>2</sub> nanoparticles on flat polymeric ultrafiltration (UF) membranes. TiO<sub>2</sub>/polymer thin film composite (TFC) reverse osmosis membranes have been investigated to mitigate biofouling by photobactericidal effect under ultraviolet (UV) radiation [13,14]. Bae and Tak [15] investigated the fouling mitigation effect of immobilized TiO<sub>2</sub> UF membranes during the activated sludge filtration. However, studies of blending membranes with nanoparticles focused primarily on gas separation [16,17] and pervaporation membranes [18,19] and have recently been extended to porous membranes for ultrafiltration (especially PVDF membranes) [9–12] and potential nanofiltration applications [20]. A search of SciFinder Scholar and Engineering Village databases has revealed the lack of studies on the use of Al<sub>2</sub>O<sub>3</sub> immobilized membranes for activated sludge filtration despite previous application to water treatment [11]. Since membrane fouling in wastewater treatment systems is instigated by biologically mediated processes that produce extracellular polymeric substances (EPS) and soluble microbial products (SMP) that are drastically different from the natural organic matter impacting fouling in water treatment. In our previous work [21], the concept of introducing Al<sub>2</sub>O<sub>3</sub> nanoparticles to PES polymer was evaluated. The effect of polymer preparation conditions such as polymer concentrations, solvent evaporation time and Al<sub>2</sub>O<sub>3</sub> nanoparticles concentrations (up to 0.05 Al<sub>2</sub>O<sub>3</sub>/PES weight ratio) in the casting solution on the membrane permeation flux were studied. The membranes morphology was characterized by SEM. Investigation of the fouling mitigation effect of Al<sub>2</sub>O<sub>3</sub> immobilized UF membranes during the activated sludge filtration was also undertaken in the previous study and revealed that Al<sub>2</sub>O<sub>3</sub>/PES membranes mitigated fouling propensity of activated sludge. Thus, the objectives of this research

\* Corresponding author. Tel.: +1 519 661 2111x85470; fax: +1 519 850 2921.

E-mail addresses: [nmaximou@uwo.ca](mailto:nmaximou@uwo.ca) (N. Maximous), [gnakhla@eng.uwo.ca](mailto:gnakhla@eng.uwo.ca) (G. Nakhla), [khwong@uwo.ca](mailto:khwong@uwo.ca) (K. Wong), [wkwan@eng.uwo.ca](mailto:wkwan@eng.uwo.ca) (W. Wan).

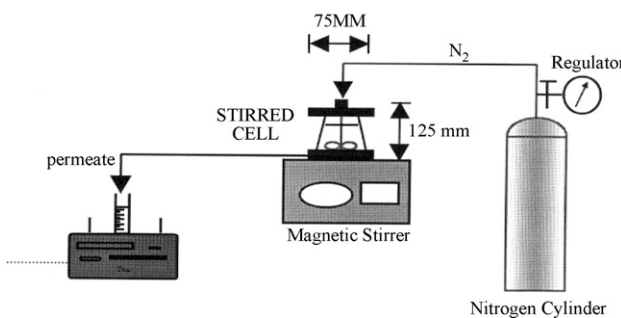


**Fig. 1.** Schematic diagram of stirred batch cell system.

include the optimization of  $\text{Al}_2\text{O}_3$  nanoparticles loading, determination of MWCO for different  $\text{Al}_2\text{O}_3/\text{PES}$  membrane and a deeper understanding of the membrane fouling mechanisms.

## 2. Experimental

### 2.1. Membrane preparation

Pure PES flat membranes were prepared by phase inversion [22]. PES Radel A-100 (Solvay Advanced Polymers, Alpharetta, GA, USA) was used as a membrane material. For the  $\text{Al}_2\text{O}_3$  entrapped membrane 0.01, 0.03, 0.05, 0.1 and 0.2  $\text{Al}_2\text{O}_3/\text{PES}$  ratios (w/w) nanoparticles with average particle size of 48 nm and a surface area of  $34 \text{ m}^2/\text{g}$  (Sigma-Aldrich Canada Ltd.) were dissolved into the N-methyl pyrrolidone (NMP) solution and the solution was sonicated at  $60^\circ\text{C}$  for 72 h to obtain a uniform and homogeneous casting suspension. Subsequently, 18 wt.% PES polymer was added and the mixture was sonicated again for a week. The membranes were cast with a 100  $\mu\text{m}$  casting knife onto a glass plate at room temperature. The nascent membrane was evaporated at  $25 \pm 1^\circ\text{C}$  for 15 s and then immersed in a deionized water coagulation bath maintained at  $18 \pm 1^\circ\text{C}$  for 2 min. For all prepared membranes, after complete coagulation, the membrane was transferred to a water bath for 15–17 days at room temperature to remove the remaining solvent from the membrane structure before testing.

### 2.2. Membrane characterization

Membrane filtration was carried out using a dead end stirred batch cell operated under constant trans-membrane TMP (Model No. 8050, Amicon) as shown in Fig. 1. The mode of constant TMP is suitable for the study of membrane fouling and is widely used for wastewater treatment [23–25]. The deionized water (DIW) flux was determined for the PES control membranes as well as the  $\text{Al}_2\text{O}_3$  entrapped PES at different TMPs of 0.345, 0.69, 1.034, 1.38 and 1.724 bar. The cross-sectional morphologies of the membranes were characterized using field-emission scanning electron microscopy (SEM, Leo 1530, LEO Electron Microscopy Ltd.) at 1 kV with no conductive coating. To expose the membrane cross-section for SEM characterization, the membranes were cryogenically fractured in liquid nitrogen. Molecular weight cut-off of the membrane was determined using polyethylene oxide (PEO),  $M_w$  100,000, 200,000, 300,000 and 600,000 aqueous solutions. The concentrations of PEO were measured using LEICA Auto ABBE refractometer model 100500B [26]. Rejection was calculated by the following equation:

$$\% R = \left( \frac{1 - C_{\text{per}}}{C_{\text{feed}}} \right) \times 100 \quad (1)$$

where  $C_{\text{per}}$  is the concentration of PEO in permeate and  $C_{\text{feed}}$  the concentration of PEO in the feed. The smallest molecular weight

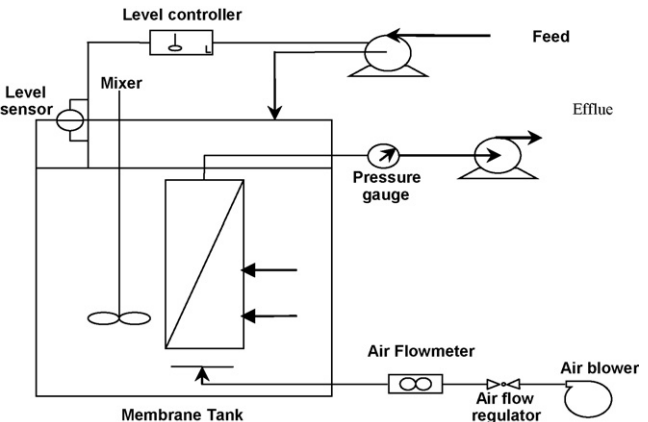


**Fig. 2.** Schematic diagram of MBR experimental setup.

that is rejected by 90% is taken as the MWCO of the membrane [26]. The MWCO is an established method to measure the pore size as the comparison with crystal structures and electron micrographs indicated that the membrane pore radius,  $R_p$ , is close to the effective hydrodynamic radius of the polymer in solution,  $R_h$ , of the largest PEG or PEO able to diffuse through the pore or to block ion conductance [27–29]. Lee et al. [30] plot the molecular weight ( $M_w$ ) dependence of radius of gyration ( $R_g$ ) for PEO, and linear fits yield the coefficient  $\nu$  in  $R_g \propto M_w^\nu$  equal to 0.515 within statistical error. According to the authors [30] the relation between the polymer  $M_w$  and  $R_g$  is presented by the following equation:

$$\log R_g = \nu \log M_w \quad (2)$$

where  $M_w$  of the polymer is in Da and  $R_g$  is in Å.

The aforementioned authors [30] indicated that PEO behaves as an ideal chain. For high molecular weight polymers in "good solvents" (such as water for PEO), mean field and renormalization group treatments of excluded volume interactions yielded  $\nu$  of 0.6 and 0.588, respectively [31]; a  $\nu$  of 0.583 has been experimentally determined for PEO in water for  $80,000 < M_w < 10^6$  [32]. The polymer theory [33] predicts for a random coil polymer in a  $\theta$  solvent (i.e., an ideal random flight chain) that:

$$R_h = 0.665 R_g \quad (3)$$

### 2.3. Activated sludge

Activated sludge used in this study was cultivated in a submerged laboratory scale MBR (Fig. 2) treating synthetic wastewater for more than 5 months. The membrane module ZeeWeed-1 (GE Water and Process Technologies, Oakville, ON, Canada) was used in this study. Starch and casein,  $(\text{NH}_4)_2\text{SO}_4$ , and  $\text{KH}_2\text{PO}_4$  were used as carbon, nitrogen and phosphorus sources, respectively. Additional nutrients and alkalinity ( $\text{NaHCO}_3$ ) were also supplied to the reactor. The feed composition and the influent wastewater characteristics are summarized in Table 1 while Table 2 presents the activated sludge characteristics.

### 2.4. Membrane fouling analysis

In order to alleviate the impact of compaction of the new polymeric membranes on flux, pre-filtration studies with pure deionized water (DIW) were conducted until a steady-state flux ( $J_{iw}$ ) was achieved. For sludge filtration, the TMP and stirring speed were kept constant at 0.69 bar (as this is a typical TMP for submerged membranes like Zenon [34]) and 600 rpm, respectively. The permeate flux was determined by monitoring the volume of permeate with time. After the filtration test, the membrane was

**Table 1**  
Feed composition and influent characteristics.

Compound	Concentration (mg/L)
Feed composition	
Casein	125
Starch	84.4
Sodium acetate	31.9
Ammonium sulfate $[(\text{NH}_4)_2\text{SO}_4]$	93.0
Magnesium sulfate $[\text{MgSO}_4 \cdot 7\text{H}_2\text{O}]$	69.6
Calcium chloride $[\text{CaCl}_2 \cdot 2\text{H}_2\text{O}]$	22.5
Potassium hydrogen phosphate $[\text{K}_2\text{HPO}_4]$	5.9
Sodium hydroxide $[\text{NaOH}]$	175.0
Ferric chloride $[\text{FeCl}_3]$	11.0
Copper sulfate $[\text{CuSO}_4 \cdot 4\text{H}_2\text{O}]$	0.08
Sodium molybdate $[\text{NaMoO}_4 \cdot 2\text{H}_2\text{O}]$	0.15
Manganese sulfate $[\text{MnSO}_4 \cdot \text{H}_2\text{O}]$	0.13
Zinc chloride $[\text{ZnCl}_2]$	0.23
Cobalt chloride $[\text{CoCl}_2 \cdot 6\text{H}_2\text{O}]$	0.42
Potassium dihydrogen phosphate $[\text{KH}_2\text{PO}_4]$	23.6
Sodium carbonate $[\text{Na}_2\text{CO}_3]$	216
Sodium bicarbonate $[\text{NaHCO}_3]$	169
Parameters	Average $\pm$ SD (# of samples)
Influent characteristics	
TSS (mg/L)	48.8 $\pm$ 9.8 (16)
TCOD (mg/L)	363.3 $\pm$ 33.5 (16)
Nitrates $[\text{NO}_3^-]$ (mg $\text{NO}_3^-$ -N/L)	0.2 $\pm$ 0.05 (16)
Ammonia $[\text{NH}_3]$ (mg $\text{NH}_3$ -N/L)	20.6 $\pm$ 4.3 (16)
Orthophosphate $[\text{PO}_4^{3-}]$ (mg $\text{PO}_4^{3-}$ -P/L)	6.1 $\pm$ 0.6 (16)

TSS: total suspended solids; TCOD: total chemical oxygen demand.

washed in a cross-flow manner with DIW, the pure DIW flux ( $J_{fw}$ ) was measured four times after this cleaning regime. The degree of membrane fouling was calculated quantitatively using the resistance in series model [35].

$$J = \frac{\text{TMP}}{\eta \cdot R_t} \quad (4)$$

where  $J$  = the flux (L/m<sup>2</sup> h); TMP = trans-membrane pressure (1.03 bar);  $\eta$  = viscosity of water at room temperature.

$$R_t = R_m + R_f + R_c \quad (5)$$

Resistances values were obtained by the following equations

$$R_m = \frac{\text{TMP}}{\eta \cdot J_{fw}} \quad (6)$$

$$R_f = \frac{\text{TMP}}{(\eta \cdot J_{fw}) - R_m} \quad (7)$$

$$R_c = \frac{\text{TMP}}{(\eta \cdot J) - (R_m + R_f)} \quad (8)$$

where  $R_m$  is the intrinsic membrane resistance;  $R_f$  is the sum of the resistances caused by solute adsorption into the membrane pores or walls and chemically reversible cake;  $R_c$  is the cake resistance formed by cake layer deposited over the membrane surface.

**Table 2**  
Sludge characteristics.

Parameters	Average $\pm$ SD (# of samples)
TSS (g/L)	8.1 $\pm$ 1.1 (24)
VSS (g/L)	5.9 $\pm$ 1.1 (24)
SCOD (mg/L)	22.4 $\pm$ 2.0 (24)
Nitrates $[\text{NO}_3^-]$ (mg $\text{NO}_3^-$ -N/L)	7.5 $\pm$ 1.6 (24)
Ammonia $[\text{NH}_3]$ (mg $\text{NH}_3$ -N/L)	1.10 $\pm$ 0.57 (24)
Orthophosphate $[\text{PO}_4^{3-}]$ (mg $\text{PO}_4^{3-}$ -P/L)	5.6 $\pm$ 1.3 (24)
pH	7.3 $\pm$ 0.2 (24)
DO	4.2 $\pm$ 0.8 (24)

DO: dissolved oxygen; TSS: total suspended solids; SCOD: soluble chemical oxygen demand; VSS: volatile suspended solids.

**Table 3**  
The Effect of  $\text{Al}_2\text{O}_3$  nanoparticles concentration on the membrane DIW permeation.

$\text{Al}_2\text{O}_3/\text{PES}$ ratio	DIW permeation (L/m <sup>2</sup> h bar) <sup>a</sup>
0.00 (PES control)	866.5 $\pm$ (59.6)
0.01	1016 $\pm$ (38)
0.03	1026 $\pm$ (18)
0.05	1268 $\pm$ (35)
0.1	727.5 $\pm$ (28.1)
0.2	284.1 $\pm$ (4.0)

<sup>a</sup> The values presented in this table are the slopes of the straight lines generated by recording the DIW flux at different TMP (0.345, 0.6895 and 1.0342 bar) with  $R^2$  values of 0.89–0.99. Numbers within parenthesis represent the 95% confidence intervals.

Membrane fouling rate was calculated by fitting the experimental data using Sigma Plot software version 10 (Systat Software, Inc., Canada). The theoretical curves were generated by previous software; the data fit the exponential decay (3-parameters) equation (Eq. (9)) with  $R^2$  of 0.90–0.99.

$$y = y^0 + ae^{-bt} \quad (9)$$

where  $y$  = permeability (L/m<sup>2</sup> h bar),  $t$  = time (h),  $y^0$  = permeability at ( $t$ ) equal infinity and  $a, b$  are the regression constants. The fouling rate was determined using Eq. (10).

$$\frac{dy}{dt} = abe^{-bt} \quad (10)$$

The initial fouling rates (representing the initial curve) for all membranes are the averages of  $dy/dt$  at five points at times varying between 0.01 and 0.05 h. However, the final fouling rates are the averages of  $dy/dt$  at five points at times varying between 2.5 and 3 h.

### 3. Results and discussion

#### 3.1. $\text{Al}_2\text{O}_3$ content

**Table 3** shows the  $\text{Al}_2\text{O}_3$ -entrapped PES membranes DIW permeation. As apparent from **Table 3**, membrane DIW permeation increased with the increase of the nanoparticles concentration in the casting solution up to 0.05  $\text{Al}_2\text{O}_3/\text{PES}$  and declined drastically for the 0.1 and 0.2  $\text{Al}_2\text{O}_3/\text{PES}$ . The maximum DIW permeability for the 0.05  $\text{Al}_2\text{O}_3/\text{PES}$  of 1268 L/m<sup>2</sup> h bar is 46% higher than the PES while the minimum of 248 L/m<sup>2</sup> h bar for the 0.2  $\text{Al}_2\text{O}_3/\text{PES}$  is 71% lower than the PES. The effect of  $\text{Al}_2\text{O}_3$  nanoparticles on membrane performance can be explained in terms of two opposing trends. Since  $\text{Al}_2\text{O}_3$  has higher affinity for water than PES, penetration velocity of water into nascent membrane increased with  $\text{Al}_2\text{O}_3$  concentration during the phase inversion. In addition, solvent diffusion from the membrane to the water can also be increased by  $\text{Al}_2\text{O}_3$  addition. Since the interaction between polymer and solvent molecules decreased due to the hindrance of nanoparticles [36], solvent molecules could diffuse more easily from the polymer matrix. On the other hand, nanoparticles may clog some of membrane pores during the phase inversion leading to decrease in the water flux. Therefore, the 0.05  $\text{Al}_2\text{O}_3/\text{PES}$  ratio load was considered the optimum load above which the clogging effect of the nanoparticles becomes predominant.

#### 3.2. Membrane characterization

The SEM pictures of the neat PES membranes and different  $\text{Al}_2\text{O}_3/\text{PES}$  membranes are shown in Fig. 3a–f. The SEM pictures show that all prepared membranes were typically UF membranes, highly porous and asymmetric with sponge-like structures. Though the structures of the membranes were not distinctively different, the higher  $\text{Al}_2\text{O}_3$  content induced aggregation and caused

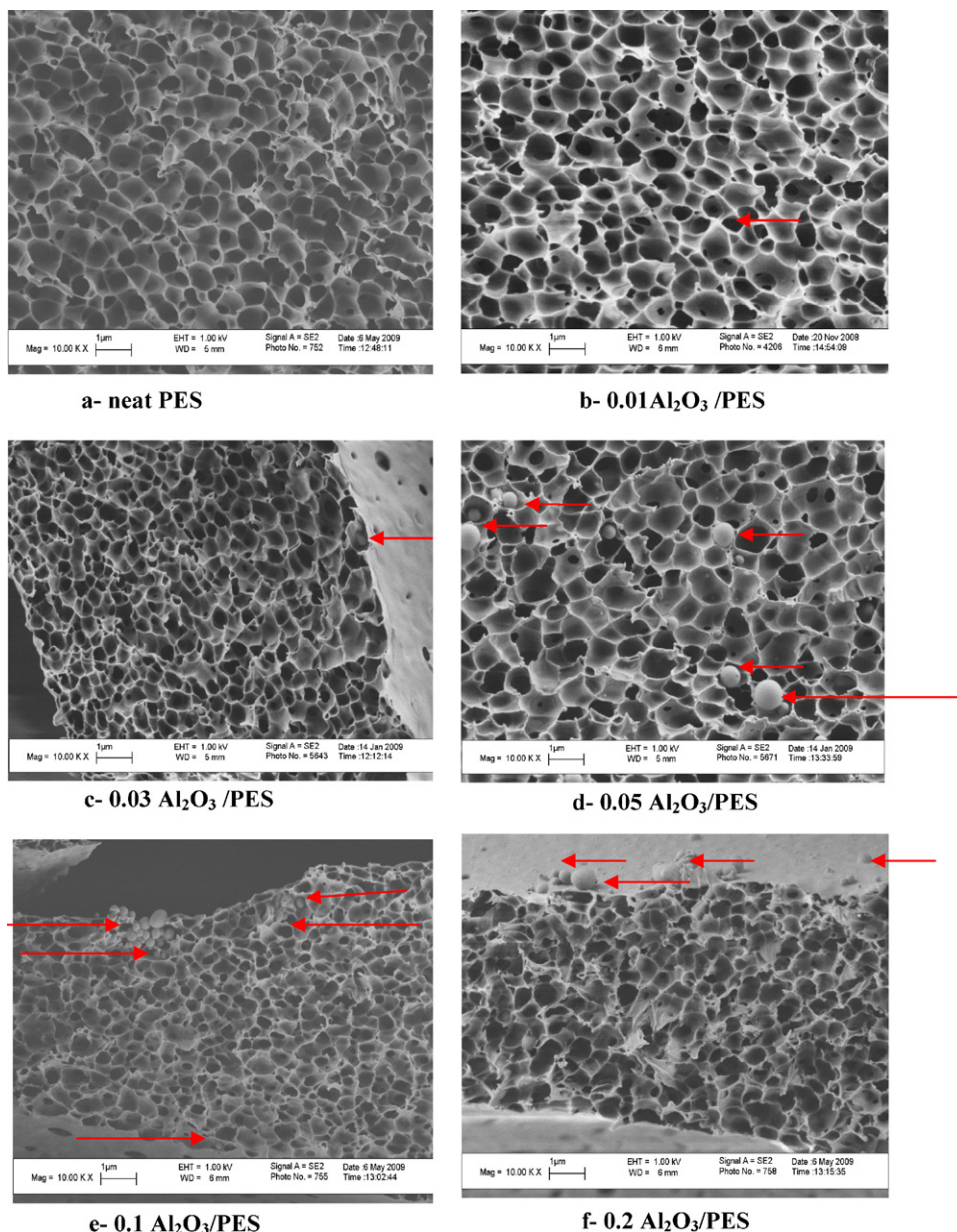


**Fig. 3.** SEM picture for the neat PES and  $\text{Al}_2\text{O}_3$ -PES membranes.

pore plugging. The number and the size of  $\text{Al}_2\text{O}_3$  nanoparticles aggregates increased with increasing  $\text{Al}_2\text{O}_3$  ratios from 0.05 to 0.2  $\text{Al}_2\text{O}_3/\text{PES}$  (Fig. 3d and f). Fig. 4 shows the MWCO of the tested membranes using PEO, the membranes pore size ranges are shown on the top of each column. As apparent from Fig. 4, the PES, 0.01 and 0.03  $\text{Al}_2\text{O}_3/\text{PES}$  have MWCO of 600 kDa. However, the 0.05, 0.1 and 0.2  $\text{Al}_2\text{O}_3/\text{PES}$  have MWCO of 200 kDa. The differences in MWCO measured for the tested membranes may be attributed to the aggregation phenomenon of  $\text{Al}_2\text{O}_3$  nanoparticles discussed above. Using Eqs. (2) and (3), the value of  $R_h$  for the PEO polymer ( $M_w = 600$  kDa) and consequently the values of  $R_p$  of the tested membranes with MWCO of 600 kDa (neat PES, 0.01 and 0.03  $\text{Al}_2\text{O}_3/\text{PES}$ ) and 200 kDa (0.05, 0.1 and 0.2  $\text{Al}_2\text{O}_3/\text{PES}$ ) were estimated to be in the range of 0.06 and 0.05  $\mu\text{m}$ , respectively, based on  $v$  of 0.515 [29] and 0.15 and 0.13  $\mu\text{m}$ , respectively, based on  $v$  of 0.583 [32]. Since the typical pore size range of ultrafiltration membranes is 0.01–0.1  $\mu\text{m}$  [37], the results further confirm the ultrafiltration characteristics of the tested membranes.

The effect of  $\text{Al}_2\text{O}_3$  nanoparticles on the membrane strength has been studied in terms of maximum TMP sustained by the tested membranes. Table 4 shows the maximum TMP sustained by PES and different  $\text{Al}_2\text{O}_3/\text{PES}$  membranes. As apparent from the table, the maximum TMP sustained by the membranes decreased by increasing the  $\text{Al}_2\text{O}_3$  load up to 0.05  $\text{Al}_2\text{O}_3/\text{PES}$ . The higher maximum TMP sustained by 0.1 and 0.2  $\text{Al}_2\text{O}_3/\text{PES}$  membranes is mainly attributed to the aggregation phenomenon discussed

**Table 4**

The effect of  $\text{Al}_2\text{O}_3$  nanoparticles concentrations on the membrane strength.

$\text{Al}_2\text{O}_3/\text{PES}$ ratio	Max. sustained TMP (bar)
0.00 (PES control)	1.724
0.01	1.724
0.03	1.034
0.05	1.034
0.1	1.724
0.2	2.068

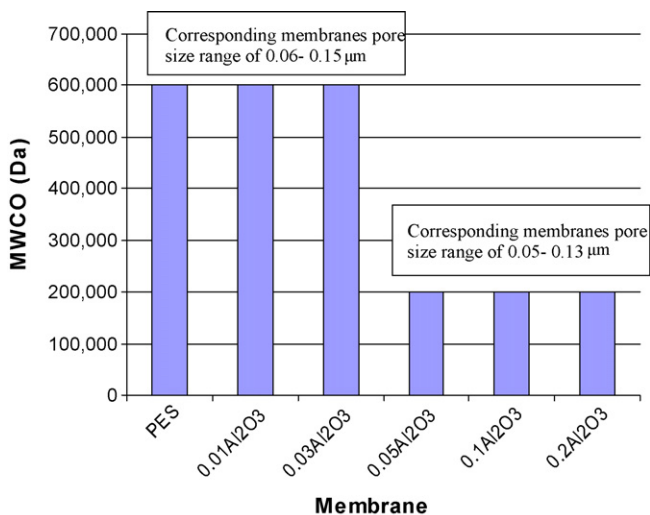


**Fig. 4.** MWCO for  $\text{Al}_2\text{O}_3$ -PES membranes using PEO.

before. Despite the fact that the maximum TMP sustained by the membrane has decreased by 40% for 0.03 and 0.05  $\text{Al}_2\text{O}_3$ /PES membranes relative to the PES control, the maximum TMP sustained by the aforementioned membranes of 1.034 bar is higher than the typical TMP (0.69 bar) for submerged membranes like Zenon [34]. Since the full-scale design of membrane modules includes packing material to increase structural integrity and resistance to pressure, it is expected that the  $\text{Al}_2\text{O}_3$ /PES membrane would sustain much higher pressures in practice.

### 3.3. Membrane fouling evaluation

#### 3.3.1. Flux decline

**Fig. 5** illustrates the temporal flux decline for PES and  $\text{Al}_2\text{O}_3$ -entrapped PES membranes using activated sludge as a feed at 20 °C

and TMP of 0.69 bar. Results presented in this paper correspond to an average of two to four replicates, with the tested membranes randomly chosen from different independent sheets. **Fig. 5** shows that the  $\text{Al}_2\text{O}_3$ -entrapped membranes have higher initial fluxes than the PES membrane. It is important to emphasize that all the observed differences between the six different membrane fluxes were statistically significant at the 95% confidence level. These results are consistent with the findings of Bae and Tak [38], who found that  $\text{TiO}_2$  entrapped PES membranes showed higher flux for sludge filtration than neat polymeric membrane.

**Fig. 6a-f** illustrates the experimental and theoretical permeability data for tested membranes for sludge filtrations. As apparent from the graphs, the permeability data are consistent with the hypothetical three-phase-process [39], comprising of initial fouling (phase 1) resulting in a rapid permeability decline mainly due to the irreversible deposition of the soluble fraction of the biomass suspension (presumably soluble microbial products, SMP), followed by deposition of sludge particles on the membrane surface and in the previously deposited layers is the main phenomenon occurring during phase 2 when the flux declines more slowly. Phase 3 is then defined when flux appears to stabilize, indicating that permeation drag and back transport have reached equilibrium. Although reduced permeation drag limits further severe fouling, compaction of the cake layer would play a significant role in the slight increase in filtration resistance observed during this last phase. As little fouling still occurs during phase 3, this operation can be maintained during a certain filtration period, before cleaning of the membrane is required [39]. **Table 5** shows the initial and final fouling rates for sludge filtrations by the tested membranes as well as the  $y^0$  values. It is noteworthy that all the observed differences in fouling rates between the two phases for each membrane were statistically significant at the 95% confidence level. Furthermore, the differences in phase 1 and phase 2 fouling rates between the tested membranes are also statistically significant at the 95% confidence levels.

It is well known that membrane fouling can be influenced by hydrodynamic conditions, such as permeation drag and back

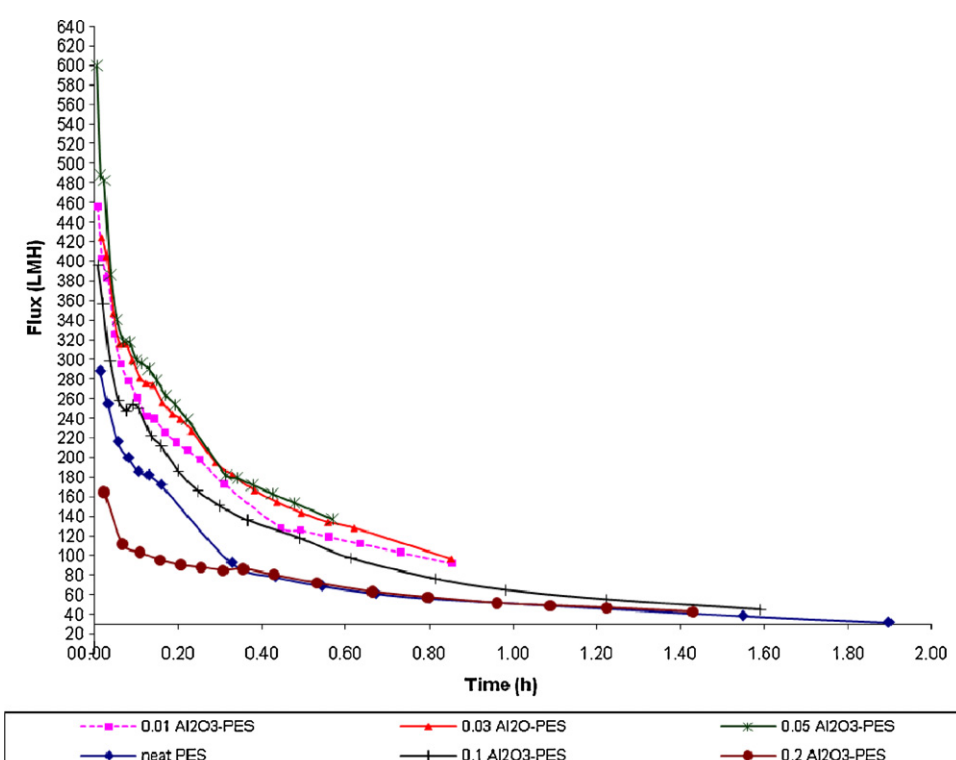


**Fig. 5.** Temporal flux decline for sludge sample at 0.69 bar.

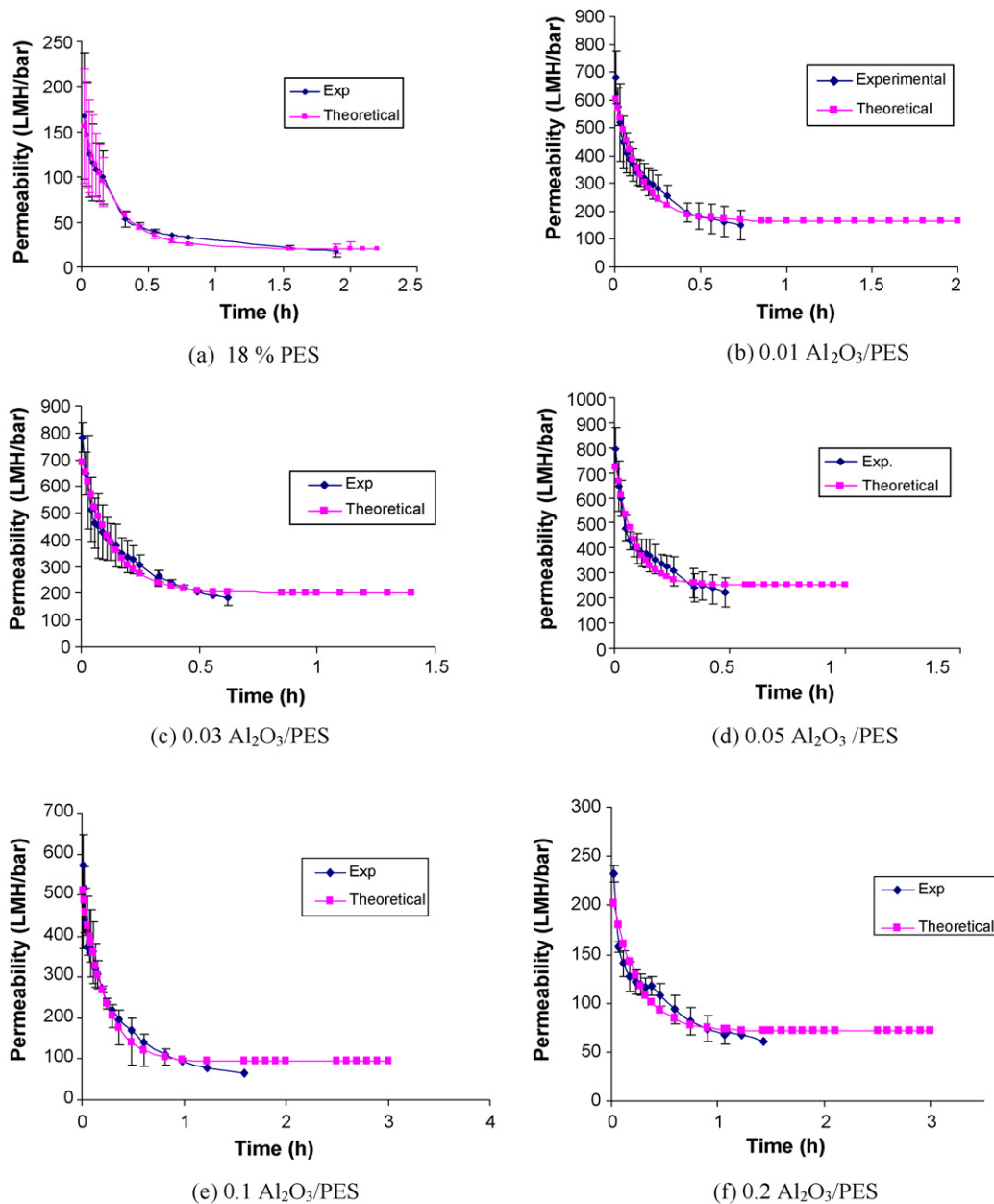


Fig. 6. Membranes permeabilities.

transport, and chemical interaction between foulants and membranes [40]. Since all the membranes were tested at the same hydrodynamic condition, the different fouling behavior could be attributed to surface properties of the membranes which were changed by nanoparticle entrapment. As apparent from Table 5, despite the higher initial fouling rate, the steady-state fouling rates of Al<sub>2</sub>O<sub>3</sub> entrapped membranes were significantly lower by 2.5, 4.5, 550, 8.25 × 10<sup>3</sup> and 4 × 10<sup>8</sup> times for 0.1, 0.2, 0.01, 0.03 and 0.05 Al<sub>2</sub>O<sub>3</sub>/PES membranes, respectively than the neat PES membrane which coupled with the 3.5–12 times higher pseudo-steady-state

permeability (Table 5) observed for the Al<sub>2</sub>O<sub>3</sub> entrapped membrane relative to the neat membrane, suggest that the surface of Al<sub>2</sub>O<sub>3</sub> entrapped membrane can be more hydrophilic than the neat polymeric membrane due to the higher affinity of metal oxides to water. Thus, the hydrophobic adsorption between sludge particles and Al<sub>2</sub>O<sub>3</sub> entrapped membrane was reduced. The steady-state permeability for sludge filtration at the optimum Al<sub>2</sub>O<sub>3</sub> loading of 5% by weight of PES was more than 12 folds the nascent PES membrane. On the other hand, for the 0.1 and 0.2 Al<sub>2</sub>O<sub>3</sub>/PES membrane, severe pore plugging was observed as confirmed by the resistance

**Table 5**

Initial and pseudo-steady-state fouling rates.

Parameters	PES	0.01 Al <sub>2</sub> O <sub>3</sub> /PES	0.03 Al <sub>2</sub> O <sub>3</sub> /PES	0.05 Al <sub>2</sub> O <sub>3</sub> /PES	0.1 Al <sub>2</sub> O <sub>3</sub> /PES	0.2 Al <sub>2</sub> O <sub>3</sub> /PES
Initial fouling rate (L/m <sup>2</sup> bar h <sup>-2</sup> )	526.2	2647.3	3301	4387	375	264.3
Pseudo-steady-state fouling rate (L/m <sup>2</sup> bar h <sup>-2</sup> )	0.005	9.09E-06	6.06E-07	1.25E-11	0.0011	0.002
Pseudo-steady-state permeability ( $\gamma^0$ ) (L/m <sup>2</sup> bar h)	20.4	166	202	252	94.5	71.6

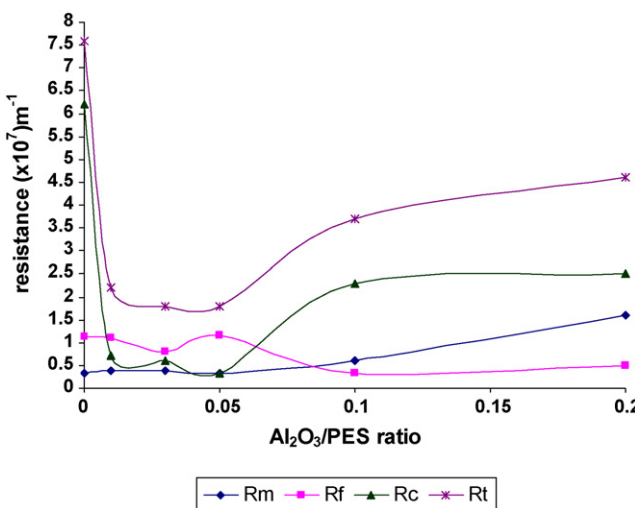


Fig. 7. Filtration resistance of neat and  $\text{Al}_2\text{O}_3$ -entrapped membranes.

in series model discussed in the next section. Since 0.05  $\text{Al}_2\text{O}_3/\text{PES}$  membranes have the lowest pseudo-steady-state fouling rate and the highest pseudo-steady-state permeability (Table 5) combined with the highest DIW permeability, it is deemed to be the optimum of the five tested loads.

### 3.3.2. Fouling mitigation and fouling mechanism of $\text{Al}_2\text{O}_3$ entrapped membranes

The impact of surface properties on cake layer resistance can be readily discerned from Fig. 7, with the differences between membrane resistances ( $R_m$ ) statistically insignificant at the 95% confidence level except for 0.1 and 0.2  $\text{Al}_2\text{O}_3/\text{PES}$  membranes. The results clearly show that  $R_c$  and  $R_t$  values decreased substantially with increasing  $\text{Al}_2\text{O}_3$  load up to 0.05  $\text{Al}_2\text{O}_3/\text{PES}$ , which coupled with the insignificant observed differences between the  $R_m$  values (up to 0.05  $\text{Al}_2\text{O}_3/\text{PES}$  ratio) for tested membranes and also the insignificant differences between  $R_f$  values at 95% confidence suggests that introducing the  $\text{Al}_2\text{O}_3$  nanoparticles might enhance PES membrane hydrophilicity. The  $R_c$  value decreased from  $6.2 \times 10^7 \text{ m}^{-1}$  in the control membrane to  $0.32 \times 10^7 \text{ m}^{-1}$  at the optimum  $\text{Al}_2\text{O}_3$  load and similarly  $R_t$  decreased from  $7.6 \times 10^7$  to  $1.8 \times 10^7 \text{ m}^{-1}$ . Furthermore, the addition of  $\text{Al}_2\text{O}_3$  up to 0.05 load reduced the contribution of the cake resistance ( $R_c$ ) to the total resistance as reflected by the  $R_c/R_t$  ratio. As apparent from Fig. 7, the  $R_c/R_t$  decreased from 82% in the neat PES to 33%, 34%, and 18% in the 0.01, 0.03, and 0.05  $\text{Al}_2\text{O}_3/\text{PES}$ , which coupled with the fact that cake resistance mainly due to extracellular polymeric substance (EPS) proved to be the predominant fouling mechanism [41], suggests that introducing the  $\text{Al}_2\text{O}_3$  nanoparticles decrease the adhesion or the adsorption of the EPS on the membrane surface. Bae and Tak [15] concluded that fouling mitigation also increased when the  $\text{TiO}_2$  entrapped-nanoparticles content increased in the polysulfone (PSF) casting solution. For the 0.1 and 0.2  $\text{Al}_2\text{O}_3/\text{PES}$  ratio, the severe pore plugging with nanoparticles is confirmed by the increase in the intrinsic membrane resistance ( $R_m$ ) from  $0.32 \times 10^7 \text{ m}^{-1}$  in the 0.05  $\text{Al}_2\text{O}_3/\text{PES}$  to  $0.61 \times 10^7$  and  $1.6 \times 10^7 \text{ m}^{-1}$ , respectively in the 0.1 and 0.2  $\text{Al}_2\text{O}_3/\text{PES}$ , as well as the dramatic decrease of  $R_f$  values relative to both the nascent PES and other  $\text{Al}_2\text{O}_3$  loadings. The decrease in  $R_f$  values for 0.1 and 0.2  $\text{Al}_2\text{O}_3/\text{PES}$  membranes can be explained as follows: Eqs. (6) and (7) show that the  $R_m$  value depends on the value of  $J_{fw}$ , while the  $R_f$  value depends on the  $J_{iw}$ . In the case of 0.1 and 0.2  $\text{Al}_2\text{O}_3/\text{PES}$  membranes, the membranes pores are already occupied with the  $\text{Al}_2\text{O}_3$  nanoparticles aggregates, as discussed in Section 3.2, hence the val-

ues of  $J_{fw}$  and  $J_{iw}$  were very close and consequently the  $R_f$  values for the two aforementioned membranes are very small. As apparent from Fig. 7, cake filtration is the predominant fouling mechanism in the neat PES, 0.1 and 0.2  $\text{Al}_2\text{O}_3/\text{PES}$  membranes with  $R_c/R_t$  ratio of 82%, 75% and 55%, respectively. This observation is in agreement with the results for the other commercial membranes of the same hydrophobic material (e.g. PM 30) and with hydrophilic material as YM 30 membranes [42].

## 4. Conclusions

This research aimed to study the optimum load of  $\text{Al}_2\text{O}_3$  nanoparticles for fouling mitigation during the activated sludge filtration and to provide better understanding of membrane fouling mechanisms. Major findings from this study are:

1. PES membrane characteristics and performances were changed by the addition of  $\text{Al}_2\text{O}_3$  nanoparticles to the casting solution, with porosity increasing and the hydrophobic interaction between the membrane surface and foulants decreasing.
2.  $\text{Al}_2\text{O}_3$  entrapped membrane showed lower flux decline during activated sludge filtration compared to neat polymeric membrane, with the pseudo-steady-state permeability increasing by 3.5 to 12 folds.
3. Although fouling mitigation initially increased with nanoparticles content, it reached an optimum limit above which pore plugging occurred resulting in dramatic changes in membrane performance. Within the 0.01, 0.03, 0.05, 0.1 and 0.2  $\text{Al}_2\text{O}_3/\text{PES}$  ratios, the 0.05  $\text{Al}_2\text{O}_3/\text{PES}$  ratio was deemed to be optimum in terms of membrane fouling mitigation.
4. For the 0.01, 0.03 and 0.05  $\text{Al}_2\text{O}_3/\text{PES}$  ratios membranes,  $R_c$  accounted for 33%, 34% and 18% of the total resistances of  $2.2 \times 10^7$ ,  $1.8 \times 10^7$  and  $1.8 \times 10^7 \text{ m}^{-1}$ , respectively with insignificant differences in  $R_f$  and  $R_m$ .
5. For the nascent PES and the highly loaded  $\text{Al}_2\text{O}_3$  membranes, i.e.; 0.1 and 0.2  $\text{Al}_2\text{O}_3/\text{PES}$ , the  $R_c/R_t$  was significantly higher at 55–82% of the total resistance of  $3.7 \times 10^7$  to  $7.6 \times 10^7 \text{ m}^{-1}$ , emphasizing the high contribution of cake resistance.
6. As the  $\text{Al}_2\text{O}_3$  load increases in the membrane matrix, the possibility of nanoparticles aggregation increased as reflected by the SEM pictures and by the decrease of membrane MWCO from 600 kDa for the neat PES, 0.01 and 0.03  $\text{Al}_2\text{O}_3/\text{PES}$  membranes to 200 kDa for 0.05, 0.1 and 0.2  $\text{Al}_2\text{O}_3/\text{PES}$ .

## Acknowledgement

The authors would like to thank Solvay Advanced Polymers, Alpharetta, GA, USA for supplying the PES polymer.

## References

- [1] P. Pandey, R.S. Chauha, Membranes for gas separation, *Prog. Polym. Sci.* 26 (2001) 853–893.
- [2] I. GennC, S. Kuypers, R. Leysen, Effect of the addition of  $\text{ZrO}_2$  to polysulfone based UF membranes, *J. Membr. Sci.* 113 (1996) 343–350.
- [3] P. Aerts, I. Genne, S. Kuypers, R. Leysen, I.F.J. Vankelecom, P.A. Jacobs, Polysulfone-aerosil composite membranes. Part 2. The influence of the addition of aerosil on the skin characteristics and membrane properties, *J. Membr. Sci.* 178 (2001) 1–11.
- [4] A. Bottino, C. Caparmelli, P. Piaggio, V. D'Asti, Preparation and properties of novel organic-inorganic porous membranes, *Sep. Purif. Technol.* 22–23 (2001) 269–275.
- [5] Z.S. Wang, T. Sasaki, M. Muramatsu, Y. Ebina, T. Tanake, L. Wang, M. Watanabe, Self-assembled multilayers of titania nanoparticles and nanosheets with polyelectrolytes, *Chem. Mater.* 15 (2003) 807–812.
- [6] R. Molinari, M. Mungari, E. Drioli, A.D. Paola, V. Loddo, L. Palmisano, M. Schiavello, Study on a photocatalytic membrane reactor for water purification, *Catal. Today* 55 (2000) 71–78.
- [7] R. Molinari, C. Grande, E. Drioli, L. Palmisano, M. Schiavello, Photocatalytic membrane reactors for degradation of organic pollutants in water, *Catal. Today* 67 (2001) 273–279.

- [8] R. Molinari, L. Palmisano, E. Drioli, M. Schiavello, Studies on various reactors configurations for coupling photocatalysis and membrane process in water purification, *J. Membr. Sci.* 206 (2002) 399–415.
- [9] A. Bottino, G. Capannelli, V. D'Asti, et al., Preparation and properties of novel organic-inorganic porous membranes, *J. Sep. Purif. Technol.* 22–23 (2001) 269–275.
- [10] A. Bottino, G. Capannelli, A. Comite, Preparation and characterization of novel porous PVDF-ZrO<sub>2</sub> composite membranes, *Desalination* 146 (2002) 35–40.
- [11] L. Yan, Y.-S. Li, C.B. Xiang, S. Xianda, Effect of nano-sized Al<sub>2</sub>O<sub>3</sub> – particle addition on PVDF ultrafiltration membrane performance, *J. Membr. Sci.* 276 (2006) 162–167.
- [12] D.J. Lin, C.L. Chang, F.M. Huang, L.P. Cheng, Effect of salt additive on the formation of microporous poly(vinylidene fluoride) membranes by phase inversion from LiClO<sub>4</sub>/water/DMF/PVDF system, *Polymer* 44 (2003) 413–422.
- [13] S.Y. Kwak, S.H. Kim, S.S. Kim, Hybrid organic/inorganic reverse osmosis (RO) membrane for bactericidal anti-fouling. 1. Preparation and characterization of TiO<sub>2</sub> nanoparticle self-assembled aromatic polyamide thin film composite (TFC) membrane, *Environ. Sci. Technol.* 35 (2001) 2388–2394.
- [14] S.H. Kim, S.Y.K. Wak, B.H. Sohn, T.H. Park, Design of TiO<sub>2</sub> nanoparticle self-assembled aromatic polyamide thin-film-composite (TFC) membrane as an approach to solve biofouling problem, *J. Membr. Sci.* 211 (2003) 157–165.
- [15] T.H. Bae, T.-M. Tak, Effect of TiO<sub>2</sub> nanoparticles on fouling mitigation of ultrafiltration membranes for activated sludge filtration, *J. Membr. Sci.* 249 (2005) 1–8.
- [16] J.M. Duval, B. Folkers, M.H.V. Mulder, G. Desgrandchamps, C.A. Smolders, Adsorbent filled membranes for gas separation. Part 1. Improvement of the gas separation properties of polymeric membranes by incorporation of microporous adsorbents, *J. Membr. Sci.* 80 (1993) 189–198.
- [17] M. Moaddeb, W.J. Koros, Gas transport properties of thin polymeric membranes in the presence of silicon dioxide particles, *J. Membr. Sci.* 125 (1997) 143–163.
- [18] J.P. Boom, I.J.M. Pünt, H. Zwijnenberg, R. de Boer, D. Bargeman, C.A. Smolders, H. Strathmann, Transport through zeolite filled polymeric membranes, *J. Membr. Sci.* 138 (1998) 237–258.
- [19] X. Chen, Z.H. Ping, Y.C. Long, Separation properties of alcohol–water mixture through silicalite-1-filled silicone rubber membranes by pervaporation, *J. Appl. Polym. Sci.* 67 (1998) 629–636.
- [20] I. Genne, W. Doyen, W. Adriansens, R. Leysen, Organo-mineral ultrafiltration membranes, *Filtr. Sep.* 34 (1997) 964–966.
- [21] N. Maximous, G. Nakhla, W. Wan, K. Wong, Preparation, characterization and performance of Al<sub>2</sub>O<sub>3</sub>/PES membrane for wastewater filtration, *J. Membr. Sci.* 341 (2009) 67–75.
- [22] T. Matsura, *Synthetic Membranes and Membrane Separation Processes*, CRC Press, Boca Raton, FL, 1994.
- [23] T. Ueda, K. Hata, Domestic wastewater treatment by a submerged membrane bioreactor with gravitational filtration, *Water Res.* 33 (1999) 2888–2892.
- [24] X. Zheng, J. Liu, Dyeing and printing wastewater treatment using a membrane bioreactor with a gravity drain, *Desalination* 190 (2006) 277–286.
- [25] X. Zheng, J.X. Liu, Optimizing of operational factors of a membrane bioreactor with gravity drain, *Water Sci. Technol.* 52 (2005) 409–416.
- [26] K.J. Kim, A.G. Fane, R. Ben Aim, M.G. Liu, G. Joansson, I.C. Tessaro, A.P. Broek, D. Bargeman, A comparative study of techniques used for porous membrane characterization: pore characterization, *J. Membr. Sci.* 87 (1994) 35–46.
- [27] O.V. Krasilnikov, R.Z. Sabirov, V.I. Ternovsky, P.G. Merzlyak, J.N. Muratkhodjaev, A simple method for the determination of the pore radius of ion channels in planar lipid bilayer-membranes, *FEMS Microbiol. Immunol.* 105 (1992) 93–100.
- [28] P.G. Merzlyak, L.N. Yuldasheva, C.G. Rodrigues, C.M.M. Carneiro, O.V. Krasilnikov, S.M. Bezrukova, Polymeric nonelectrolytes to probe pore geometry: application to the a-toxin trans membrane channel, *J. Biophys.* 77 (1999) 3023–3033.
- [29] T.K. Rostovtseva, E.M. Nestorovich, S.M. Bezrukova, Partitioning of differently sized poly(ethylene glycol)s into OmpF porin, *J. Biophys.* 82 (2002) 160–169.
- [30] H. Lee, R.M. Venable, A.D. MacKerell Jr., R.W. Pastor, Molecular dynamics studies of polyethylene oxide and polyethylene glycol: hydrodynamic radius and shape anisotropy, *J. Biophys.* 95 (2008) 1590–1599.
- [31] M. Doi, S.F. Edwards, *The Theory of Polymer Dynamics*, Clarendon Press, Oxford, 1986.
- [32] K. Devanand, J.C. Selser, Asymptotic-behavior and long-range interactions in aqueous-solutions of poly (ethylene oxide), *Macromolecules* 24 (1991) 5943–5947.
- [33] C. Tanford, *Physical Chemistry of Macromolecules*, John Wiley & Sons, New York, 1961.
- [34] S. Arabi, G. Nakhla, Impact of calcium on the membrane fouling in membrane bioreactors, *J. Membr. Sci.* 314 (2008) 134–142.
- [35] M. Mulder, *Basic Principles of Membrane Technology*, Kluwer Academic Publishers, 1996, p. 383.
- [36] I.C. Kim, K.H. Lee, T.M. Tak, Preparation and characterization of integrally skinned uncharged polyetherimide asymmetric nanofiltration membrane, *J. Membr. Sci.* 183 (2001) 235–247.
- [37] M.C. Porter, *Handbook of Industrial Membrane Technology*, Noyes Publications, Park Ridge, New Jersey, USA, 1990, p. 155–156.
- [38] T.H. Bae, T.-M. Tak, Interpretation of fouling characteristics of ultrafiltration membrane during the filtration of membrane bioreactor mixed liquor, *J. Membr. Sci.* 264 (2005) 151–160.
- [39] S.P. Hong, T.H. Bae, T.M. Tak, S. Hong, A. Randall, Fouling control in activated sludge submerged hollow fiber membrane bioreactor, *Desalination* 143 (2002) 219–228.
- [40] E. Tardieu, A. Grasmick, V. Geaugey, J. Manem, Influence of hydrodynamics on fouling velocity in a recirculated MBR for wastewater treatment, *J. Membr. Sci.* 156 (1999) 131–140.
- [41] N. Maximous, S. Arabi, M. Kim, G. Nakhla, Comparison of biofoulants in BNR-MBR and conventional MBR (C-MBR) systems, in: WEFTEC conference, McCormick Place Chicago, IL, October 18–22, 2008.
- [42] N. Maximous, G. Nakhla, W. Wan, Comparative assessment of hydrophobic and hydrophilic membrane fouling in wastewater applications, *J. Membr. Sci.* 339 (2009) 93–99.